

## Supplemental Data

### Transducer-Based Force Generation

#### Explains Active Process

#### in *Drosophila* Hearing

Björn Nadrowski, Jörg T. Albert, and Martin C. Göpfert

### Supplemental Experimental Procedures

#### Model description

Our model posits that each transducer population comprises  $N$  parallel transduction modules, with each module comprising one ion channel that serially couples to one gating spring and  $n$  adaptation motors. The channel is either open or closed, with both states being separated by an intrinsic energy difference  $\Delta G$ . The gating spring has stiffness  $\kappa$  and extension  $l$ . Connecting to the channel's gate, this spring shortens by a distance  $d$  (the gating swing) as the channel opens. For the anterior and posterior transducer population, the position of the motors on their support is given by  $x_{a,p}$ . The motors display a linear force-velocity relation,  $\xi_a \dot{X}_{a,p} = -f_0 + f_{mot}$ , where  $\xi_a$  characterizes the slope of the relation,  $f_{mot}$  is the elastic force imposed by the gating spring, and  $f_0$  is the force the motors generate at stall. This stall force is assumed to linearly depend on the open probability  $P_o$  of the channels [1].

Displacements of the receiver  $X$  are related to displacements of the transducer modules by a geometric projection factor  $\gamma$ . Because this factor is not known, we project all the movements and forces arising at the molecular level to the level of the receiver. The projected gating

spring stiffness reads  $K_{GS} = N\gamma^2\kappa$ , the projected gating swing is  $D = d/\gamma$ , and the motor position translates to  $X_{a,p} = x_{a,p}/\gamma$ . Forces scale with  $\gamma$ , distances with  $1/\gamma$ , leading to the force-velocity relation for all the  $N$  transduction modules of one transducer population  $\lambda_a \dot{X}_{a,p} = -F_0 + F_{mot}$ , with  $\lambda_a = N\gamma^2\xi_a$ , and  $F_{mot} = K_{GS}(X - X_a)$  (anterior population) and  $F_{mot} = K_{GS}(X - X_p)$  (posterior population). Energies, including the energy required to open a single transduction channel [2],

$$E_G = \frac{1}{2}\kappa d^2 = \frac{1}{2}K_{GS}D^2/N, \text{ do not scale.}$$

The harmonic oscillator that represents the sound receiver is described by an effective mass  $m$ , a linear stiffness  $K_{AJ}$ , and friction  $\lambda$ , with stiffness and friction arising from the receiver's proximal suspension by Johnston's organ and the antennal joint [3]. A static displacement,  $X$ , of the receiver by an external force is balanced by the combined elastic forces of this joint and the gating springs. In steady state, the extensions of the gating springs of the anterior and posterior neural population,  $Y_a$  and  $Y_p$ , and the position of the receiver,  $X$ , satisfy the relation  $F_{ext} = -K_{GS}Y_p + K_{GS}Y_a + K_{AJ}X$ . The average extensions of the springs of the two transducer populations are  $Y_p = -X - X_p - DP_o(-X - X_p)$  and  $Y_a = X - X_a - DP_o(X - X_a)$ . The open probability  $P_o$  can be written as [4, 5]

$$P_o(Y) = \frac{1}{1 + A \exp[-Y/\delta]} \quad (1)$$

$$\delta = \frac{Nk_B T}{K_{GS}D}, \quad (2)$$

where  $\delta$  is the typical distance the receiver has to move in order to change the state of the channels,  $A = \exp\left[\frac{(\Delta G + K_{GS}D^2/(2N))}{(k_B T)}\right]$  is a factor that accounts for the intrinsic energy difference between the channel states,  $\Delta G$ , and  $k_B$  and  $T$  denote the Boltzmann constant and the ambient temperature, respectively. The dynamics of the system are described by four first-order coupled differential equations:

$$\dot{X} = V \quad (3)$$

$$m\dot{V} = -K_{GS}(X - X_a - DP_o(X - X_a)) + K_{GS}(-X - X_p - DP_o(-X - X_p)) - \lambda V - K_{AJ}X + F_{ext} \quad (4)$$

$$\lambda_a \dot{X}_a = K_{GS}(X - X_a - DP_o(X - X_a)) + F_{max}(SP_o(X - X_a) - 1) \quad (5)$$

$$\lambda_a \dot{X}_p = K_{GS}(-X - X_p - DP_o(-X - X_p)) + F_{max}(SP_o(-X - X_p) - 1). \quad (6)$$

Equation 4 couples the harmonic oscillator determined by friction  $\lambda$ , mass  $m$  and stiffness  $K_{AJ}$  to the molecular motors via the gating-springs of stiffness  $K_{GS}$ . The dynamics of the collections of motors of the anterior and posterior transducer population is described by equations 5-6. In the absence of an external load, these motors develop the constant velocity  $F_{max} / \lambda_a$ . We further introduce a dimensionless parameter  $S$  that characterizes the coupling strength between channel open probabilities and the force-velocity characteristics of the motors [1]:  $F_0 = F_{max}(1 - SP_o)$ . The stall force  $F_0$  is maximal when the channels are closed ( $F_0 = F_{max}$ ), and minimal when the channels are open ( $F_0 = F_{max}(1 - S)$ ).

Note that Equations 3 and 4 can be easily transformed into one second-order equation by simply replacing  $V$  with  $\dot{X}$  and  $\dot{V}$  with  $\ddot{X}$  in Equation 4. In the special case of a stationary open probability  $P_{o,S} = 0.5$

(see below), both motor populations move sympathetically with  $X_p = -X_a - 2\delta \ln A$ , meaning that either Equation 5 or Equation 6 would suffice to describe the temporal evolution of both motor populations, thereby simplifying our model to two coupled differential equations.

### Stationary points

The model equations 3-6 can be used to analytically determine the stationary points of the system. These stationary points are given by the following relations:

$$X_s = \frac{F_{ext}}{K_{AJ}} \quad (7)$$

$$X_{p,S} = -2X_s + X_{a,S} \quad (8)$$

where  $X_{a,S}$  is a solution of

$$P_{o,S} = P_o(X_s - X_{a,S}) = \frac{K_{GS}(X_s - X_{a,S}) - F_{max}}{K_{GS}D - F_{max}S}. \quad (9)$$

Equation 9 shows that the system can have 1 to 3 stationary states, two of which can be stable, leading to the bistable state in the state diagram (Figure 4F).

### Scaling invariances

The performance of the model (equations 3-6) does not depend on the individual values of  $\Delta G, F_{max}$ , and  $S$ , because given values of  $\Delta G, S, F_{max}$  can be replaced by  $\Delta G \rightarrow \Delta G + \Delta G'$ ,  $F_{max} \rightarrow F_{max} (1 + \Delta G' \delta K_{GS} / (F_{max} k_B T))$  and

$S \rightarrow S / (1 + \Delta G' \delta K_{GS} / (F_{\max} k_B T))$ , without affecting the temporal evolution of channel open probabilities, receiver displacements, and relative motor displacements. The only difference is a different gating spring tension at rest, as the stationary value of  $X_{a,S}$  (and  $X_{p,S}$ ) changes according to  $X_{a,S} \rightarrow X_{a,S} - \Delta G' \delta / (k_B T)$ . Because we cannot measure absolute gating spring tensions and motor positions, absolute values of  $\Delta G, F_{\max}$ , and  $S$  are arbitrary, whereas the value of  $F_{\max} S$  is not.

### Linear response function

To determine the linear response function (Figure 3A), we actuated the sound receiver with a multi-sine stimulus consisting of  $n_{stim}$  sinusoids of identical force amplitude  $A$  and distinct frequencies  $f_i$ :

$$F_{ext} = \sum_{i=1}^{n_{stim}} A \cos(2\pi f_i t).$$

For each stimulus frequency, we determined the

Fourier transforms of the stimulus force  $\tilde{F}_{ext}(f_i)$  and the phase-locked displacement response  $\tilde{X}(f_i)$ . Fourier transforms of a given time-

dependent quantity  $Q(t)$  were calculated as  $\tilde{Q}(f) = \int_{-\infty}^{\infty} \exp[i2\pi ft] Q(t) dt$ . The

amplitude of the response function  $|\tilde{\chi}(f)| = |\tilde{X}(f) / \tilde{F}_{ext}(f)|$  can be regarded

as the force-dependent sensitivity of the system at frequency  $f$ . For

small stimuli,  $\tilde{\chi}(f)$  was independent of the forcing amplitude, defining

the linear response function  $\tilde{\chi}_0(f) = \lim_{F_{ext} \rightarrow 0} \tilde{\chi}(f)$ .

### Activity

As stated in the main text, we deduce the power contribution of the active elements from the difference between the dissipated power  $\bar{P}_D$  and the stimulus power  $\bar{P}_S$ . The results depicted in Figure 3B are obtained using the fit parameter  $\lambda$  from the general fit:

$$\bar{P}_D = -1/T_s \int_0^{T_s} \lambda \bar{X}^2 dt, \text{ neglecting dissipation by the transduction modules. In}$$

order to quantify this internal dissipation, we used the fit parameter  $\lambda_a$  of the general fit as an estimate of motor friction; this description is justified by the fact that, for a passive system with  $S = 0$ , the transduction modules behave like simple dashpots with friction  $\lambda_a$  and Hookean springs. The dissipated power then reads

$$\bar{P}_D = -1/T_s \int_0^{T_s} \lambda \bar{X}^2 + \lambda_a \bar{X}_a^2 + \lambda_a \bar{X}_p^2 dt, \text{ resulting in an increased power gain}$$

that remains positive for all stimulus intensities (Figure 4C).

### Displacement-force cycles

The average displacement-force cycles (Figure 3C) have been deduced from the multisine-stimulus data used to calculate the linear response function (Figure 3A). Using Fourier transforms, all stimulus frequencies except one were removed before calculating phase-locked average displacements and forces. Simulations were performed using single-sine stimuli.

### Free fluctuations (Figure 3D)

The influence of stochastic forces on the movements of the sound receiver was taken into account by adding noise terms to equations 3-6. The resulting equations read [1]:

$$\dot{X} = V \quad (10)$$

$$m\dot{V} = -K_{GS}(X - X_a - DP_o(X - X_a)) + K_{GS}(-X - X_p - DP_o(-X - X_p)) - \lambda V - K_{AJ}X + F_{ext} + \eta \quad (11)$$

$$\lambda_a \dot{X}_a = K_{GS}(X - X_a - DP_o(X - X_a)) + F_{max}(SP_o(X - X_a) - 1) + \eta_a \quad (12)$$

$$\lambda_a \dot{X}_p = K_{GS}(-X - X_p - DP_o(-X - X_p)) + F_{max}(SP_o(-X - X_p) - 1) + \eta_p, \quad (13)$$

where  $\eta, \eta_a$  and  $\eta_p$  have zero mean, with their respective characteristics being given by the autocorrelation functions  $\langle \eta(t)\eta(0) \rangle, \langle \eta_a(t)\eta_a(0) \rangle$  and  $\langle \eta_p(t)\eta_p(0) \rangle$ . For simplicity, we assume that noise sources are uncorrelated and that noise is Gaussian. Because of the explicit symmetry of our model, the motor noise  $\eta_a$  and  $\eta_p$  share the same characteristics. The noise sources giving rise to  $\eta$  are Brownian motion of air molecules hitting the receiver and thermal transitions between the open and closed states of the channels. This channel clatter exerts stochastic forces on the receiver via the gating-springs. Assuming that the time constant of the channel clatter is short compared to the other time constants of the system, the fluctuation-dissipation theorem yields  $\langle \eta(t)\eta(0) \rangle = 2k_B T \lambda \delta(t)$  [1]. The characterization of  $\eta_a$  is less simple since it reflects fluctuations of thermal origin and contributions of active motor movements [1]. For simplicity, we also used the fluctuation-dissipation theorem to estimate  $\eta_a$ :

$\langle \eta_a(t)\eta_a(0) \rangle = 2k_B T \lambda_a \delta(t)$ . Note that the set of stochastic differential equations 10-13 obeys the fluctuation-dissipation theorem if  $S = 0$ .

### Fluctuation-dissipation theorem (Figure 3E)

The fluctuation-dissipation theorem asserts that for a system in thermal equilibrium, the spectral density of the free fluctuations  $\tilde{C}(f)$  is linearly related to the imaginary part of the linear response function  $\tilde{\chi}''(f)$ :

$$\tilde{C}(f) = 2k_B T \frac{\tilde{X}_0''(f)}{2\pi f}, \quad (14)$$

where  $T$  is the ambient temperature [6]. The 'effective temperature' at which the system would satisfy the fluctuation-dissipation theorem can thus be written as  $T_{eff}(f) = \frac{2\pi f \tilde{C}(f)}{2k_B \tilde{\chi}''(f)}$  [1, 6]. A system in thermal equilibrium will satisfy the fluctuation-dissipation theorem,  $T_{eff}/T = 1$ , at all frequencies.

### Phase-Locking (Figure 4B)

Actuating the sound receiver with a sinusoidal stimulus  $F_{ext}(t)$  at frequency  $f_s$  induces a peak in the receiver's power spectrum. We defined the degree of phase-locking as the ratio between the power contained in this phase-locked peak and the system's total power [6] in a frequency band between 100 Hz and  $2f_s$ :

$$R = \frac{\sqrt{\int_{100}^{2f_s} \frac{\tilde{C}_x(f_s)}{\tilde{C}_s(f_s)} \tilde{C}_s(f) df}}{\sqrt{\int_{100}^{2f_s} \tilde{C}_x(f) df}}. \quad (15)$$

Here,  $\tilde{C}_x(f) = \int_{-\infty}^{\infty} \langle X(t)X(0) \rangle \exp[i2\pi f t] dt$  is the sound receiver's power

spectral density under the influence of the sinusoidal stimulus, and  $\tilde{C}_s(f_s)$  is the corresponding spectral density of the stimulus force. The frequency band was chosen to eliminate harmonics and low-frequency components caused by background noise.

### **Excess open probability (Figures 2A, 4D,E)**

The excess open probability was calculated as

$P_e = \max(P_{o,a} - P_{o,s}, 0) + \max(P_{o,p} - P_{o,s}, 0)$ , where  $P_{o,a}, P_{o,p}$  denote the open probabilities of the anterior and posterior channel populations, respectively, and  $P_{o,s}$  is the open probability at rest.

### **Deviations between analytical calculations and noisy simulations**

Analytically calculated linear response functions (Figure 3A) and spectral densities (Figure 3D) display slightly higher values than those obtained by noisy simulations. This deviation results from stochastic forces that push the system into the nonlinear region where mechanical sensitivity is decreased (Figure 4A).

### **Fitting procedure**

We have fitted the series of steps by numerically integrating the deterministic system defined by equations 3-6, using

$P_{o,S}, S, K_{AJ}, K_{GS}, \delta, \lambda, \lambda_a, m$  and  $N$  as fit parameters. The model parameters  $D$  and  $F_{\max}$  were calculated using equations 2 and 9.

Individual fits were performed by numerically integrating equations 3-6 for a single force step of given amplitude and polarity and by comparing predicted and measured receiver displacements. Measurement points used for the fits were distributed logarithmically, gradually decreasing the density of points from the beginning to the end of the step. The cost-function used for individual fits was

$$\sum_{j=1}^{N_{FS}} \frac{(S_j - Y_j)^2}{N_{FS}}, \quad (16)$$

where  $N_{FS}$  is the number of the measurement points and  $S_j$  and  $Y_j$  are simulated and measured receiver displacements.

General fits were performed by simultaneously fitting displacement responses to 10 small force steps (peak displacements < 397-737 nm and force amplitudes < 3.6 - 39 pN,  $N=7$ ), the linear response function, and the spectral density of free fluctuations. To enhance the speed of the fitting procedure, the linear response function of the model was calculated analytically for the noiseless system using equations 3-6. Similarly, the spectral density of the model's free fluctuations was calculated analytically using the noise sources defined above (see section "Free fluctuations") in conjunction with the linear response function.

The cost-function of the general fit was

$$\begin{aligned}
 & \left[ \sum_{i=1}^{N_S} \frac{\sum_{j=1}^{N_{i,FS}} \left( \frac{S_{i,j} - Y_{i,j}}{E_{S,i,j}} \right)^2}{N_{i,FS}} \frac{1}{P_i^2} \frac{\sum_{i=1}^{N_S} P_i^2}{N_S} \right] \\
 & + \frac{\sum_{k=1}^{N_\chi} \left( \frac{\tilde{\chi}'_{0,C}(f_k) - \tilde{\chi}'_0(f_k)}{E_{\chi',k}} \right)^2}{N_\chi} + \frac{\sum_{k=1}^{N_\chi} \left( \frac{\tilde{\chi}''_{0,C}(f_k) - \tilde{\chi}''_0(f_k)}{E_{\chi'',k}} \right)^2}{N_\chi} \\
 & + \frac{\sum_{l=1}^{N_C} \left( \frac{\tilde{C}_C(f_l) - \tilde{C}(f_l)}{E_{C,l}} \right)^2}{N_C}.
 \end{aligned} \tag{17}$$

Here,  $N_S = 10$  is the number of force steps,  $N_{i,FS}$  is the number of measured points in step  $i$ ,  $S_{i,j}$  and  $Y_{i,j}$  are the simulated and measured receiver displacements for point  $j$  and step  $i$ , and  $P_i$  is the peak displacement in response to step  $i$ . Furthermore,  $\tilde{\chi}_{0,C}$  is the linear response function calculated using equations 3-6,  $N_\chi$  is the number of points used for fitting the linear response function,  $\tilde{C}_C(f)$  is the analytically calculated spectral density, and  $N_C$  the number of points used for fitting the spectral density. Because large steps consistently displayed higher sums of squared residuals than small ones, step responses were normalized to squared peak displacement amplitudes  $P_i^2$ . For each experiment (ensemble of step responses, linear response function, free fluctuations), in turn, the sum of the squared residuals was normalized to the number of measurement points, ensuring that all the different experiments were similarly weighted by the general fit.

Initial parameter values used for individual fits were those obtained by the general fit. In order to find local minima of the cost-functions, we used the Nelder Mead Simplex algorithm implemented in the Gnu Scientific Library.

### Force estimation

The noncontact electrostatic actuation of the sound receiver (see materials and methods) resulted in a linear relation between initial receiver acceleration  $\ddot{X}$  and command voltage  $V_C$  in the range of displacements which were used for the general fit [7]:  $\ddot{X} = aV_C$ . The applied force therefore reads  $F_{ext} = m\ddot{X} = amV_C$ . For each receiver, we determined  $a$  using the initial acceleration and the command voltage of the 10 force steps used for the general fit. Note that equations 3-6 are invariant with respect to a scaling of  $F_{ext}, K_{GS}, K_{AJ}, \lambda, \lambda_a, m, N$  by a constant factor. The stochastic differential equations 10-13, however, are not invariant with respect to such scaling, which means that by simultaneously fitting step responses, the linear response function, and also the spectral density of free fluctuations, unambiguous estimates of the parameter values of  $F_{ext}, K_{GS}, K_{AJ}, \lambda, \lambda_a, m, N$  are obtained.

### Time constants

In a quiescent system, the dynamical variables  $V, X, X_a, X_p$  approach the positions given by the stationary state. When only one of these variables is dislocated from the stationary point while the others remain fixed, the relaxation of this variable to its stationary position can be described, to linear order, by a single exponential and an associated

relaxation time constant. The relaxation time constant  $\tau_a$  of the position of the molecular motors [8] can be calculated using eqs. 5 or 16, yielding

$$\tau_a = \frac{\lambda_a}{K_{GS} \left( 1 - \frac{D}{\delta} \left( 1 - \frac{SF_{\max}}{K_{GS}D} \right) P_o (1 - P_o) \right)}. \quad (18)$$

Similarly, we can attribute a relaxation time constant to the position of the receiver's tip. Let us first consider the fly's ear as a system in which the inertia of the receiver is negligible. In this case, eq. 3 becomes obsolete and eq. 4 reads

$$\lambda \dot{X} = -K_{GS} (X - X_a - DP_o (X - X_a)) + K_{GS} (-X - X_p - DP_o (-X - X_p)) - K_{AJ} X + F_{ext}. \quad (19)$$

The relaxation time constant  $\tau_{ml}$  of the receiver of this 'massless' system thus can be written as

$$\tau_{ml} = \frac{\lambda}{K_{AJ} + 2K_{GS} \left( 1 - \frac{D}{\delta} P_o (1 - P_o) \right)}. \quad (20)$$

Our model, however, takes inertial effects into account, describing the position  $X$  of the receiver by a second order differential equation. With respect to relaxation times, three different scenarios can be distinguished: the underdamped case, critical damping, and the overdamped case. According to general fit parameter values, the return of the fly's receiver to its stationary position falls into the underdamped case, displaying a damped oscillation at frequency

$f_{ud} = \sqrt{(1/\tau_{ud})(2/\tau_{ml} - 1/\tau_{ud})}/(2\pi)$  and an exponentially decaying amplitude characterized by the time constant

$$\tau_{ud} = \frac{2m}{\lambda}. \quad (21)$$

For all flies examined,  $\tau_{ud}$  was substantially shorter than  $\tau_a$  (Table S2), meaning that the observable relaxation of the receiver is dominated by the slow relaxation of the adaptation motors.

## Supplemental References

1. Nadrowski, B., Martin, P., and Jülicher, F. (2004). Active hair-bundle motility harnesses noise to operate near an optimum of mechanosensitivity. *Proc. Natl. Acad. Sci. USA* *101*, 12195-12200.
2. Albert, J.T., Nadrowski, B., and Göpfert, M.C. (2007). Mechanical signatures of transducer gating in the *Drosophila* ear. *Curr. Biol.* *17*, 1000-1006.
3. Göpfert, M.C., Humphris, A.D.L., Albert, J.T., Robert, D., and Hendrich, O. (2005). Power gain exhibited by motile mechanosensory neurons in *Drosophila* ears. *Proc. Natl. Acad. Sci. USA* *102*, 325-330.
4. Howard, J., and Hudspeth, A.J. (1988). Compliance of the hair bundle associated with gating of mechano-electrical transduction channels in the bullfrog's saccular hair cell. *Neuron* *1*, 189-199.
5. Hudspeth, A.J., Choe, Y., Mehta, A.D., and Martin, P. (2000). Putting ion channels to work: Mechano-electrical transduction, adaptation, and amplification by hair cells. *Proc. Natl. Acad. Sci. USA* *97*, 11765-11772.
6. Martin, P., Hudspeth, A.J., and Jülicher, F. (2001). Comparison of a hair bundle's spontaneous oscillations with its response to

mechanical stimulation reveals the underlying active process.  
Proc. Natl. Acad. Sci. USA *98*, 14380-14385.

7. Albert, J.T., Nadrowski, B., and Göpfert, M.C. (2007). *Drosophila* mechanotransduction - linking proteins and functions. *Fly* *1*, 238-241.
8. Tinevez, J.-Y., Jülicher, F., and Martin, P. (2007). Unifying the various incarnations of active hair-bundle motility by the vertebrate hair cell. *Biophys. J.* *93*, 4053-4067.

Table S1. General Fit Parameters

Parameter	fly 1	fly 2	fly 3	fly 4	Fly 5	fly 6	fly 7	mean $\pm$ 1 s.d.
$K_{GS}$ (pN/nm)	0.037	0,017	0.087	0.038	0.016	0.026	0.036	0.037 $\pm$ 0.024
$K_{AJ}$ (pN/nm)	0.040	0,032	0.084	0.053	0.026	0.017	0.037	0.041 $\pm$ 0.022
$S$	0.38	0.25	0.16	0.29	0.38	0.21	0.24	0.27 $\pm$ 0.08
$P_{o,s}$	0.50	0.58	0.50	0.50	0.50	0.50	0.50	0.51 $\pm$ 0.03
$\delta$ (nm)	223	210	239	190	208	461	246	254 $\pm$ 93
$N$	2653	1221	6823	2033	1006	6989	3031	3394 $\pm$ 2505
$\lambda$ ( $10^{-9}$ kg/s)	5.07	7.13	14.8	6.94	6.25	2.51	7.47	7.17 $\pm$ 3.76
$\lambda_a$ ( $10^{-9}$ kg/s)	99.0	10.8	42.8	117	64.4	243	90.0	95.3 $\pm$ 74.5
$m$ ( $10^{-12}$ kg)	3.57	2.7	6.99	5.44	4.8	1.93	4.39	4.29 $\pm$ 1.70

$K_{GS}$ : combined gating spring stiffness;  $K_{AJ}$ : linear elasticity of Johnston's organ and the antennal joint;  $S$ : feedback constant;  $P_{o,s}$ : stationary channel open probability;  $\delta$ : typical displacement of the receiver required to change the state of the channels;  $N$ : number of ion channels per transducer population;  $\lambda$ : receiver friction;  $\lambda_a$ : motor friction;  $m$ : apparanet mass of the receiver. For parameter definitions, see Supplemental Data.

Table S2. Derived quantities

Parameter	fly 1	fly 2	fly 3	fly 4	fly 5	fly 6	fly 7	mean $\pm$ 1 s.d.
$\tau_{ud}$ (ms)	1.48	0.76	0.95	1.57	1.54	1.54	1.18	1.28 $\pm$ 0.33
$\tau_a$ (ms)	9.30	4.00	7.32	8.23	5.40	11.7	8.48	7.77 $\pm$ 2.52
$D$ (nm)	1290	1346	1310	1112	1202	2329	1374	1423 $\pm$ 409
$F_{\max}$ (pN)	101	41.8	227	85.3	41.4	134	100	104 $\pm$ 63
$F_{\max}S$ (pN)	38.0	10.6	36.2	24.4	15.9	28.3	24.4	25.4 $\pm$ 10.0
$E_G (k_B T)$	2.90	3.20	2.74	2.93	2.89	2.53	2.79	2.85 $\pm$ 0.21

$\tau_{ud}$ : relaxation time constant of the receiver;  $\tau_a$ : relaxation time constant of the adaptation motors;  $D$ : gating swing of the channels;  $F_{\max}$ : maximal stall force of the adaptation motors;  $F_{\max}S$ : strength of the feedback between channels and motors;  $E_G$ : mechanical energy required to open a single transduction channel. For parameter definitions, see Supplemental Data.

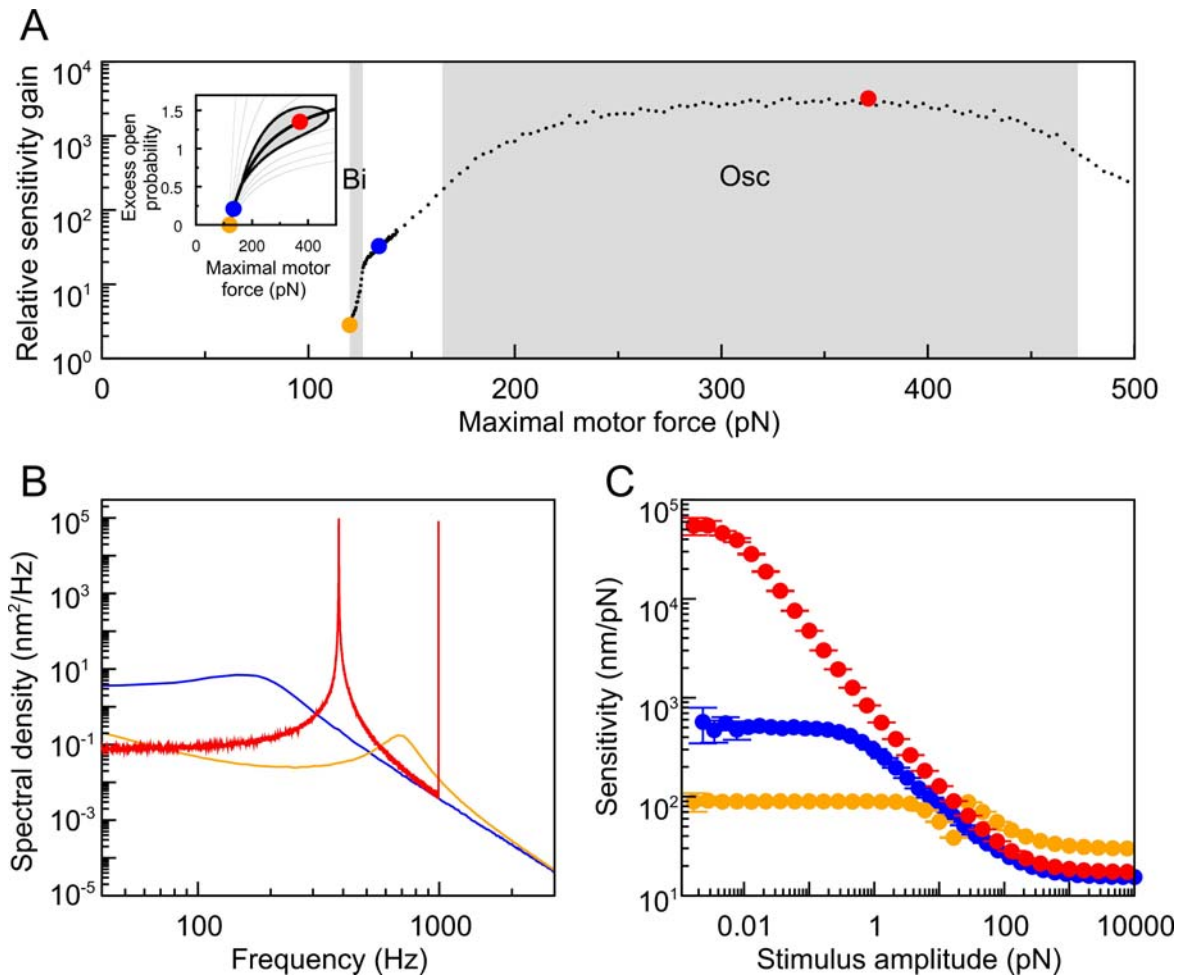


**Figure S1.** System behaviour for different dynamic states. (A)

Simulated sensitivity gain as a function of the maximal motor force.

The sensitivity gain refers to the ratio of the mechanical sensitivities of the linear regimes observed at low and high stimulus amplitudes (see also panel C). The maximal motor force ( $F_{\text{max}}$ , Supplemental Data), in turn, refers to the stall force the motors generate if the channels are closed. All parameter values correspond to those of the general fit except for  $F_{\text{max}}$  and the feedback constant  $S$ , which were varied in order

to follow the  $P_o = 0.5$  line in the state diagram (inset, same as Figure 4F). Blue circle:  $S = 0.21$  and  $F_{\max} = 134$  pN as obtained by the general fit. Orange circle: passive system with no feedback:  $S = 0$ ,  $F_{\max} = 120$  pN. Red Circle: Maximum relative sensitivity gain:  $S = 1.35$ ,  $F_{\max} = 371$  pN. Grey areas indicate the bistable regime (BI) and the oscillatory regime (OSC), respectively. **(B)** Power spectral density of free fluctuations obtained for the points depicted in **(A)**. In the case of the oscillating system, a peak at three times the fundamental frequency can be seen; the first harmonic is absent due to symmetry ( $P_o = 0.5$ ). **(C)** Corresponding mechanical sensitivity (colour code as in **(A)**) for stimulation at that frequency at which the spectral density in panel **(B)** peaks. Note the discontinuity displayed by the bistable system with no feedback (orange symbols): at low intensities, the system operates in the vicinity of one stable state, whereas it switches between both stable states at high stimulus intensities. Error bars: standard deviations obtained for six independent noisy simulations. Unless otherwise stated, all parameter values refer to fly 6 from Table S1.